Journal of Cleaner Production 234 (2019) 494–502

Contents lists available at ScienceDirect

Journal of Cleaner Production

journal homepage: www.elsevier.com/locate/jclepro

# Optimization of microwave roasting-acid leaching process for vanadium extraction from shale via response surface methodology

Yizhong Yuan [a, b, c, d, *], Yimin Zhang [a, b, c, d, e, **], Tao Liu [a, b, c, d], Pengcheng Hu [a, b, c, d], Qiushi Zheng [a, b, c, d]

[a] School of Resource and Environmental Engineering, Wuhan University of Science and Technology, Wuhan, 430081, Hubei Province, China
[b] State Environmental Protection Key Laboratory of Mineral Metallurgical Resources Utilization and Pollution Control, Wuhan University of Science and Technology, Wuhan, 430081, Hubei Province, China
[c] Hubei Collaborative Innovation Center for High Efficient Utilization of Vanadium Resources, Wuhan University of Science and Technology, Wuhan, 430081, Hubei Province, China
[d] Hubei Provincial Engineering Technology Research Center of High Efficient Cleaning Utilization for Shale Vanadium Resource, Wuhan University of Science and Technology, Wuhan, 430081, Hubei Province, China
[e] School of Resource and Environmental Engineering, Wuhan University of Technology, Wuhan, 430070, Hubei Province, China

ARTICLE INFO

*Article history:*
Received 27 September 2018
Received in revised form
19 June 2019
Accepted 23 June 2019
Available online 24 June 2019

Handling editor. Prof. Jiri Jaromir Klemeš

*Keywords:*
Vanadium-bearing shale
Microwave roasting
Response surface methodology
Enhancement mechanism

ABSTRACT

In this work, Microwave roasting (MR) was used in vanadium (V) extraction from shale for its cleanness and high efficiency. Response surface methodology (RSM) was used to optimize conditions for MR-acid leaching, the enhancement mechanism of MR for V oxidization and structural distortion of muscovite were investigated using density functional theory (DFT) and a variety of micro-Characterization methods. A Box-Behnken experimental design has been used to monitor the V extraction characteristics, as affected by MR temperature, MR time, $H_2SO_4$ concentration and leaching time. In the optimized conditions, a V leaching efficiency of 93.4% was reached. Compared with conventional roasting (CR)-acid leaching technique, MR technique had absolute advantages, its roasting temperature was reduced by 115 °C, roasting time was reduced by 32 min, $H_2SO_4$ concentration was reduced by 10%v/v and leaching time was reduced by 4 h. Selective thermal effect of MR enhanced activations of coal and pyrite and results in cracking of particles, promoting the oxidation of low-valent V. MR had an absolute advantage in dehydroxylation of muscovite, resulting the spacing expansion of Al–O(OH) octahedral structure layer as about 1.3 times as that of CR and significantly enhancing the release of V.



## 1. Introduction

Vanadium (V) is an important rare element widely used in many fields (such as V-bearing alloy steel, V catalyst, V redox flow battery et al.) due to its special alloy and catalytic properties (Hu et al., 2018a,b; Li et al., 2017; In-Hyeok Choi et al., 2018). V-bearing shale is a unique and abundant V resource in China, with an estimated reserve of approximately 61.88 billion tons (Xue et al., 2017; Li et al., 2014; X.Y. Zhang et al., 2011). Therefore, with the increasing demand for V-bearing products, V extraction form shale has been given substantial and continuous attention. However, the average grade of V (in the form of $V_2O_5$) in shale is usually less than 1 wt% and most V stably exists as isomorphism state in low valence in octahedral structure of mica-group minerals (muscovite, illite, phlogopite et al.) replacing Al (Wang et al., 2014; Zhang et al., 2013). Therefore, to extract V from shale, roasting process is necessary for breaking structure of mica-group minerals and oxidizing low-valent V (Hu et al., 2012; Zhu et al., 2012; Liu et al., 2010). Traditional sodium salt roasting-water leaching process is a well-known method to extraction V form shale. However, due to low extraction efficiency and environmental pollution, it is gradually being replaced by blank roasting-acid leaching process (Fu, 2009; Zhu et al., 2010).

As an effective and environmentally friendly technique, the use of microwave in the mineral, metallurgy and chemistry fields has

* Corresponding author. School of Resource and Environmental Engineering, Wuhan University of Science and Technology, Wuhan 430081, Hubei Province, China.
** Corresponding author. School of Resource and Environmental Engineering, Wuhan University of Technology, Wuhan, 430070, Hubei Province, China.
*E-mail addresses:* yyz2038@163.com (Y. Yuan), zym126135@126.com (Y. Zhang).

https://doi.org/10.1016/j.jclepro.2019.06.271
0959-6526/

shifted into the focus of attention in recent years (Kaewwichit et al., 2017; Wang et al., 2018; Asomaning et al., 2018). Compared to conventional heating (CR), microwave heating (MR) offers several advantages such as selective heating, rapid heating, and volumetric heating. Especially, the selective heating property plays an important role in the field of microwave applications (Lee et al., 2016; Wang et al., 2017). Up to present, some works have been made to research the effect of MR in V extraction from shale and the results show that it is more efficient than CR (Yuan et al., 2017; Yuan et al., 2016; Zhang et al., 2011). However, few researches of the optimization of MR-acid leaching process have been carried out and the enhancement mechanism of MR has not been explored thoroughly, especially the role of selective heating property of microwave plays in this enhancement mechanism has never been explored.

Response surface methodology (RSM) is a statistical and mathematical model which is widely used to design experiments and optimize process conditions (Ghafarzadeh et al., 2017; Ranic et al., 2014; Mohammed et al., 2017). RSM determines the effect of independent variables on the process and generates a mathematical model that accurately describes the process (Wang et al., 2016). It leads the experiments rapidly and efficiently along a path of improvement toward the general vicinity of the optimum (Markandeya et al., 2017). Therefore, the main advantages of RSM are reducing numbers of potential tests, making experiments less laborious and lowering the overall cost of research. However, RSM used to design experiments and optimize conditions for MR-acid leaching process in V extraction from shale has rarely been reported.

In our previous works (Yuan et al., 2016), the influences of MR temperature, MR time, microwave power, $H_2SO_4$ concentration of leaching agent, leaching temperature and leaching time on V leaching efficiency were investigated via single facts experiments. The findings showed that MR temperature, MR time, $H_2SO_4$ concentration of leaching agent, leaching temperature and leaching time were the main influence factors on V leaching efficiency. Before 100 °C (approximate boiling temperature of leaching solution), V leaching efficiency increased linearly with the increase of leaching temperature. Thus, in order to prevent the sharp evaporation of leaching solution, 95 °C is usually chosen for the appropriate leaching temperature (Hu et al., 2018; Li et al., 2018; Wang et al., 2015). Therefore, in this work, the factors including MR temperature, MR socking time, $H_2SO_4$ concentration and leaching time were systemically analysed using a Box-Behnken design (BBD) combined with response surface methodology. A mathematical model was established to describe the MR-acid leaching process for V extraction from shale and optimize the process conditions. Compared with the full factor design method, BBD combined with response surface methodology can reveal the influence of different factors on V leaching efficiency with a small number of experiments. On the other hand, by comparing with CR, the enhancement mechanism of MR for structural distortion of muscovite and V oxidization were investigated using density functional theory (DFT) with XRD, FTIR and SEM-EDS analyses of pure muscovite.

## 2. Experimental

### 2.1. Materials

The V-bearing shale used in this work was obtained from Tongshan, Hubei Province, China. The raw sample was firstly crushed to 0–3 mm by a jaw crusher (XPC-60 × 100) and a roll crusher (HLXPS-φ250 × 150).

### 2.2. Procedures

#### 2.2.1. Roasting-acid leaching experiments

The MR experiments were carried out using a HAMiLab-V microwave furnace with fixed condition of microwave power 1000 W. When the temperature reached set value, the equipment automatically cuts off the microwave source, and the material was in the heat preservation state. When the temperature was lower than the set value, the equipment would automatically start the magnetron to maintain the material temperature at the set value. The CR experiments were carried out in a SX2-10-13 muffle furnace. All of the experiments were conducted under fixed condition of heating rate 8 °C/min. The roasted samples were dry grinded less than 0.074 mm accounted for more than 75% by a vibration mill (HLXZM-100). The grounded roasted samples were leached in an SZCL-2A type magnetic and controlling temperature stirrer. The leaching experiments were conducted under fixed conditions of leaching liquid solid ratio 1.5 mL/g, leaching temperature 95 °C. The sulphuric acid used is the superior pure sulphuric acid produced by China National Pharmaceutical Group. All the experiments were carried out three or more odd times, and the standard deviation was within 2% positive or negative.

#### 2.2.2. Experimental design and statistical analysis

The experimental domain was defined taking into account the results obtained in our previous single facts experiments (Yuan et al., 2016), as well as the melting points of minerals, the operational limits of the instrument and all significant parameters in MR-acid leaching process were chosen as independent variables: MR temperature ($A = 700–900$ °C), MR time ($B = 20–40$ min), $H_2SO_4$ concentration ($C = 15–25$%v/v) and leaching time ($D = 4–8$ h). Factors and their levels are shown in Table 1, and a Box-Behnken design of experiments conducted via Design-Expert 8.0 software is displayed in Table 2. Evaluated response $Y$ (%) is V leaching efficiency of the roasted samples. Using Box-Behnken design combined with response surface methodology, only 29 experiments were needed to obtain the conclusions of 81 experiments (The total number of experiments for 4 variables and 3 levels).

The model equation of response (Y) of four independent variables was given in the following equation:

$$Y = \beta_0 + \sum_{i=1}^{4} \beta_i X_i + \sum_{i=1}^{4} \beta_{ii} X_i^2 + \sum_{i=1}^{3} \sum_{j=i+1}^{4} \beta_{ij} X_i X_j \quad (1)$$

where Y was the dependent variable, $\beta_0$ was the constant coefficient, $\beta_i$ was the coefficient of linear effect, $\beta_{ii}$ was coefficient the of quadratic effect, $\beta_{ij}$ was the coefficient of interaction effect.

All the experimental data analysis were operated on Design-Expert software. After input the experimental results, Design-Expert software could analyze the data systematically: (1). Response surface models could be fitted by means of leastsquares calculation (Eq. (1)) on Design-Expert software. (2). Design-Expert software could give some important coefficients by the analysis of variance (ANOVA) for response surface, like Values of "Prob. > F", precision and correlation coefficient, "Pred R-squared ($R^2$)" and

**Table 1**
Levels and codes of factors for Box-Behnken design.

| Factors | Symbol | Unit | Low | High | Value of code |
|---|---|---|---|---|---|
| MR temperature | $A$ | °C | 700 | 900 | −1 = 700; 0 = 800; 1 = 900 |
| MR time | $B$ | min | 20 | 40 | −1 = 20; 0 = 30; 1 = 40 |
| $H_2SO_4$ concentration | $C$ | %v/v | 15 | 25 | −1 = 15; 0 = 20; 1 = 25 |
| Leaching time | $D$ | h | 4 | 8 | −1 = 4; 0 = 6; 1 = 8 |

**Table 2**
The results of the designed experiments.

| Run | *A* | *B* | *C* | *D* | Leaching efficiency of V (*Y*) |
|---|---|---|---|---|---|
| 1 | 0 | 1 | 1 | 0 | 87.3 |
| 2 | 0 | 0 | 0 | 0 | 88.2 |
| 3 | −1 | 0 | 0 | 1 | 78.3 |
| 4 | −1 | 0 | −1 | 0 | 62.6 |
| 5 | 0 | 0 | −1 | 1 | 83.2 |
| 6 | 0 | 0 | 0 | 0 | 89.2 |
| 7 | −1 | 1 | 0 | 0 | 74.3 |
| 8 | 1 | −1 | 0 | 0 | 82.4 |
| 9 | 0 | 1 | 0 | 1 | 83.3 |
| 10 | 0 | 0 | 0 | 0 | 89.9 |
| 11 | 0 | 0 | −1 | −1 | 73.2 |
| 12 | 0 | 1 | −1 | 0 | 72.7 |
| 13 | 1 | 0 | 0 | −1 | 74.5 |
| 14 | 0 | 1 | 0 | −1 | 77.6 |
| 15 | 0 | 0 | 0 | 0 | 88.3 |
| 16 | 0 | −1 | 0 | 1 | 84.3 |
| 17 | 1 | 0 | 0 | 1 | 78.1 |
| 18 | 1 | 0 | 1 | 0 | 80.1 |
| 19 | 0 | −1 | 0 | −1 | 81.3 |
| 20 | −1 | −1 | 0 | 0 | 67.9 |
| 21 | 0 | −1 | −1 | 0 | 79.4 |
| 22 | 0 | 30 | 0 | 0 | 90.1 |
| 23 | −1 | 0 | 0 | −1 | 73.3 |
| 24 | 1 | 0 | −1 | 0 | 74.2 |
| 25 | −1 | 0 | 1 | 0 | 82.2 |
| 26 | 1 | 1 | 0 | 0 | 72.6 |
| 27 | 0 | −1 | 1 | 0 | 89.3 |
| 28 | 0 | 0 | 1 | −1 | 91.1 |
| 29 | 0 | 0 | 1 | 1 | 94.2 |

"Adj R-squared ($R^2_{adj}$). These coefficients could estimate which factors are the significant model terms and if the fitted model can be used to navigate the design space. (3). Design-Expert software could give the three-dimensional response surface and contour plots of the relationship between the dependent variables and the independent variables. These figures could help us assess the double interactive effects of the independent variables on the dependent variables (Wang et al., 2017).

### 2.3. Analytical methods

Main chemical analyses were conducted using an IRIS Advantage Radial Inductive Coupled Plasma Emission Spectrometer (ICP-AES) made by ThemoElemental Instrument Company, USA.

XRD analyses were conducted using an Empyrean X-ray Diffractometer made by PANalytical Company, Netherlands. The test conditions are: Cu Target Kalpha, scanning speed 15 deg/min, scanning range 5–90 deg, tube voltage 40 kV, tube current 40 mA.

EPMA analysis was conducted by a JXA-8230 electron probe made by JOEL Company, Japan.

FTIR analyses were conducted using a VERTEX-70 Fourier Transform Instrument made by Bruker Company, Germany. The scanning wavenumber range was 4000–400 $cm^{-1}$ and samples were pressed by KBr.

SEM-EDS analyses were conducted using a JSM-IT300 Scanning Electron Microscope Equipped made by JOEL Company, Japan with an INCAx-act Energy Spectrum Analyzer made by OXFORD Company, UK.

In this work, the structural parameters along the c axis of TOT units of muscovite before and after dehydroxylation were calculated by density functional theory (DFT). The DFT calculations were performed with the Vienna ab initio simulation package developed for periodical systems. The exchange-correlation functional used the Perdew-Burke-Ernzerhof (PBE)-version of the generalized gradient approximation and the plane-wave basis set used projector augmented waves. In detail, the tested kinetic energy cutoff value of 800 eV and a $(8 \times 4 \times 2)$ Γ-point centered k-points mesh were accomplished to truncate the plane-wave basis in the high-precision calculations of muscovite model. Full geometry optimization calculations were performed in which all structural parameters were relaxed without constraint of the space group symmetry. Namely, the space group was P1. ALL calculations were convergent until the total energy change of 10−4 eV and residual forces of 0.05 eV/Å, respectively. With these parameters, converged total energies and lattice vectors were obtained (Zheng et al., 2017).

The V content of leaching solution was measured in accordance with Chinese standard GB/T 8704.5–2007. The V leaching efficiency was calculated by equation (2):

$$\alpha_V = \frac{C_{Vl'} \times V_{l'}}{C_{Vs'} \times M_{s'}} \quad (2)$$

where $C_{Vl'}$ is the V content of the leaching solution, $V_{l'}$ is the volume of the leaching solution, $C_{Vs'}$ is the V content of the roasted sample, $M_{s'}$ is the mass of the roasted sample.

## 3. Results and discussions

### 3.1. Material characterization

The main chemical composition, XRD analysis, main mineral composition and EPMA analysis of the V-bearing shale used in this work have been reported in our previous article (Yuan et al., 2016), specific charts will no longer presented in this paper.

According to the characterization of raw sample, $V_2O_5$ grade of the shale was 0.72 wt% and most of the V was in muscovite. It was a typical low grade mica-type V-bearing shale, which was highly difficult to extract V. As for this shale, the key for V extraction is to achieve muscovite structure dissociation and V oxidation. Therefore, the calculating and characterizing the crystal lattice of pure muscovite is essential for revealing the effect of microwave roasting on V extraction. There was about 13 wt% coal and 7 wt% pyrite in the raw sample and it ensures the raw sample has fast heating fate in microwave field, because coal and pyrite belong to strong microwave absorbing medium (Forster et al., 2015; Haque, 1999).

### 3.2. Statistical analysis and model fitting

According to Box-Behnken design of experiments, all of the 29 experiments were conducted in corresponding conditions and the results were presented in Table 2. Based on the experimental data, a quadratic model with interdependent terms for two-way interaction of variables for predicting the maximum V leaching efficiency is given by software as equation (3) and the analysis of variance (ANOVA) is presented in Table 3.

$$Y = -980.35 + 2.06A + 5.20B + 11.04C + 11.22D\text{-}0.01AB\text{-}0.01AC\text{-}0.01AD + 0.02BC + 0.03BD\text{-}0.17CD\text{-}0.01A^2\text{-}0.05B^2\text{-}0.10C^2\text{-}0.52D^2 \quad (3)$$

According to Table 3, the Model F-value of 38.22 implies the model was significant. Lack of Fit F-value of 5.20 implies that it was not significant relative to the pure error (Mohammed et al., 2017). Values of "Prob > F" less than 0.05 indicates model terms were significant. The Model Prob > F value is less than 0.0001 implies that the quadratic model was significant. The other significant model terms were *A*, *B*, *C*, *D*, *AB*, *AC*, $A^2$, $B^2$, $C^2$, $D^2$, with the corresponding Prob > F values of 0.0018, 0.0150, <0.0001, 0.0002, 0.0004, 0.0015, <0.0001, <0.0001, 0.0032, 0.0092. Therefore, an equation just including the most important variables in the confidence of 95% to simplify the whole equation (3) is shown as

**Table 3**
ANOVA for response surface quadratic model.

| Source | Sum of Squares | df | Mean Square | F Value | Prob > F | significance |
|---|---|---|---|---|---|---|
| Model | 1638.61 | 14 | 117.04 | 38.22 | <0.0001 | significant |
| *A* | 45.12 | 1 | 45.12 | 14.74 | 0.0018 | |
| *B* | 23.52 | 1 | 23.52 | 7.68 | 0.0150 | |
| *C* | 519.56 | 1 | 519.56 | 169.66 | <0.0001 | |
| *D* | 77.37 | 1 | 77.37 | 25.26 | 0.0002 | |
| *AB* | 66.18 | 1 | 66.18 | 21.61 | 0.0004 | |
| *AC* | 47.13 | 1 | 47.13 | 15.39 | 0.0015 | |
| *AD* | 0.43 | 1 | 0.43 | 0.14 | 0.7138 | |
| *BC* | 5.45 | 1 | 5.45 | 1.78 | 0.2034 | |
| *BD* | 1.82 | 1 | 1.82 | 0.60 | 0.4533 | |
| *CD* | 11.76 | 1 | 11.76 | 3.84 | 0.0702 | |
| $A^2$ | 796.89 | 1 | 796.89 | 260.22 | <0.0001 | |
| $B^2$ | 137.26 | 1 | 137.26 | 44.82 | <0.0001 | |
| $C^2$ | 38.54 | 1 | 38.54 | 12.59 | 0.0032 | |
| $D^2$ | 27.90 | 1 | 27.90 | 9.11 | 0.0092 | |
| Residual | 42.87 | 14 | 3.06 | | | |
| Lack of Fit | 39.81 | 10 | 3.98 | 5.20 | 0.0631 | not significant |
| Pure Error | 3.06 | 4 | 0.77 | | | |
| Cor Total | 1681.48 | 28 | | | | |

$R^2 = 0.9745; R^2_{adj} = 0.9490$

equation (4). The $R^2$ and $R^2_{adj}$ (adjusted $R^2$) values are 0.9745 and 0.9490, respectively. The $R^2$ and $R^2_{adj}$ values are high enough and comparable. It indicates that the given quadratic response surface model sufficiently described the experimental data.

$$Y = -980.35 + 2.06A + 5.20B + 11.04C + 11.22D\text{-}0.01AB\text{-}0.01AC\text{-}0.01A^2\text{-}0.05B^2\text{-}0.10C^2\text{-}0.52D^2 \quad (4)$$

### 3.3. Model validation

To further evaluate the adequacy of the given quadratic model in fitting the experimental data of MR-acid leaching process, some important diagnostic plots (Normal% Probability against Internally Studentized Residuals, Internally Studentized Residuals against Predicted, Internally Studentized Residuals against Run Number and Predicted against Actual) were established and are showed in Fig. 1.

As shown in plot of Normal% Probability against Internally Studentized Residuals, the points are distributed approximately along with a straight line. It indicates that the error terms were normally distributed and independent of each. In plots of Internally Studentized Residuals against Predicted and Internally Studentized Residuals against Run Number, The points distributed randomly around zero on the outlier T axis and between −3.0 and + 3.0, which suggests that the quadratic model successfully established the relationship between the main variables of MR-acid leaching process and V leaching efficiency. In plot of Predicted against Actual, the points are distributed in a straight line pasting the origin with a slope of 1, which indicates that the quadratic model could predict the actual value accurately.

Fig. 2 illustrates the effects and interactions of the variables in relation to V leaching efficiency via 3D response surface plots. According to the shape of the response surface plots and their projection contour map, the significance of the influence of variables can be judged. As far as the effect of single variable is concerned, roasting temperature, socking time and $H_2SO_4$ concentration could cause obvious change of V leaching efficiency. The effect of leaching time on was less than that of other factors. As showed in Fig. 2 (a), the value of V leaching efficiency increased with the growth of roasting temperature and socking time, then decreased gradually after it reached to the top degree. It implied that this kind of shale was sensitive to temperature, suitable roasting temperature and socking time were beneficial to V leaching, but excessive temperature and time are adverse to V leaching. Unlike the previous two variables, there was always a positive correlation between $H_2SO_4$ concentration and V leaching efficiency. The steep surfaces of Fig.2 (a) and Fig.2 (b) imply the significant interactions of roasting temperature and socking time, roasting temperature and $H_2SO_4$

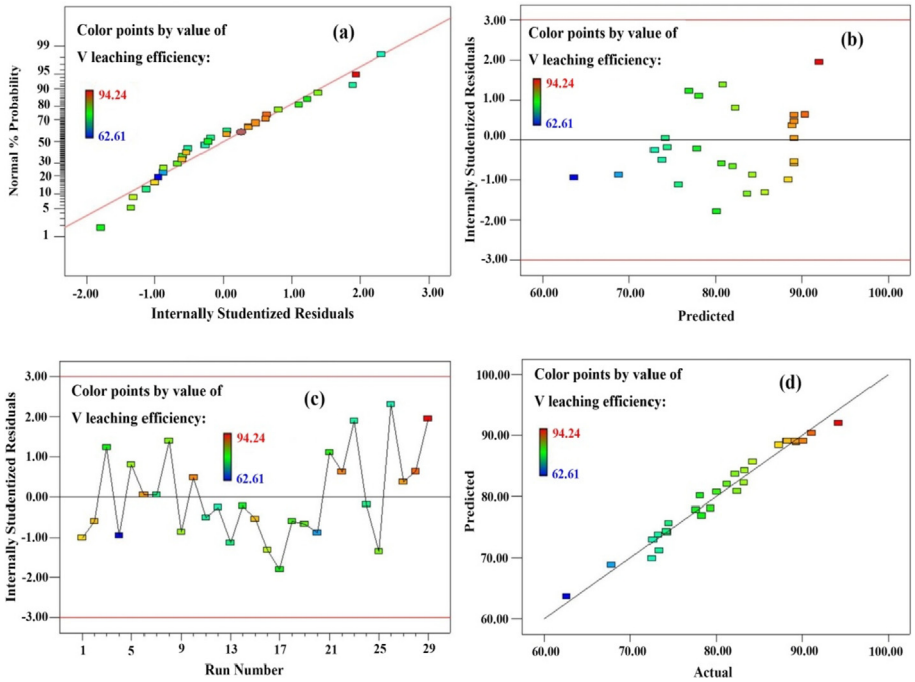


**Fig. 1.** Diagnostic plots of quadratic model. (a-Normal% Probability against Internally Studentized Residuals; b-Internally Studentized Residuals against Predicted; c-Internally Studentized Residuals against Run Number; d-Predicted against Actual).

concentration to V leaching efficiency. According to the other plots, the interactions of roasting temperature and leaching time (Fig. 2 (c)), socking time and $H_2SO_4$ concentration (Fig. 2 (d)), socking time and leaching time (Fig. 2 (e)), $H_2SO_4$ concentration and leaching time (Fig. 2 (f)) were not significant.

### 3.4. Optimization and comparison

According to the model validation above, the quadratic model (Eq. (1)) can accurately describe the MR-acid leaching process of V-bearing shale. Based on the model, taking the highest V leaching rate as an optimization target, software generated 24 solutions as presented in Table 4.

In the suggested 24 solutions, V leaching efficiencies were all more than 93% with a gap of less than 1%, the corresponding $H_2SO_4$ concentrations were almost 25%v/v. Therefore, it was not appropriate to choose optimized conditions only based on the V leaching efficiency or $H_2SO_4$ concentration. Taking the energy consumption and process efficiency into consideration, the solution No.23 was selected with the minimum roasting temperature (785.84 °C), minimum roasting time (28.82 min) and last second short leaching time (5.94 h). Practical verification experiments were carried out in the adjusted conditions of MR temperature 785 °C, MR time 28 min, $H_2SO_4$ concentration 25%v/v and leaching time 6 h. The result was 93.4%, which was only 0.2 percentage points higher than the predicted value.

Based on the experiments of CR-acid leaching process, when the V leaching efficiency was 93.8% (close to optimized result in MR-acid leaching process), the CR temperature was 900 °C, CR time was 60 min, $H_2SO_4$ concentration was 35%v/v and leaching time was 10 h. It is obvious that MR had a significant promoting effect on V extraction from V-bearing shale. The comparison of the main

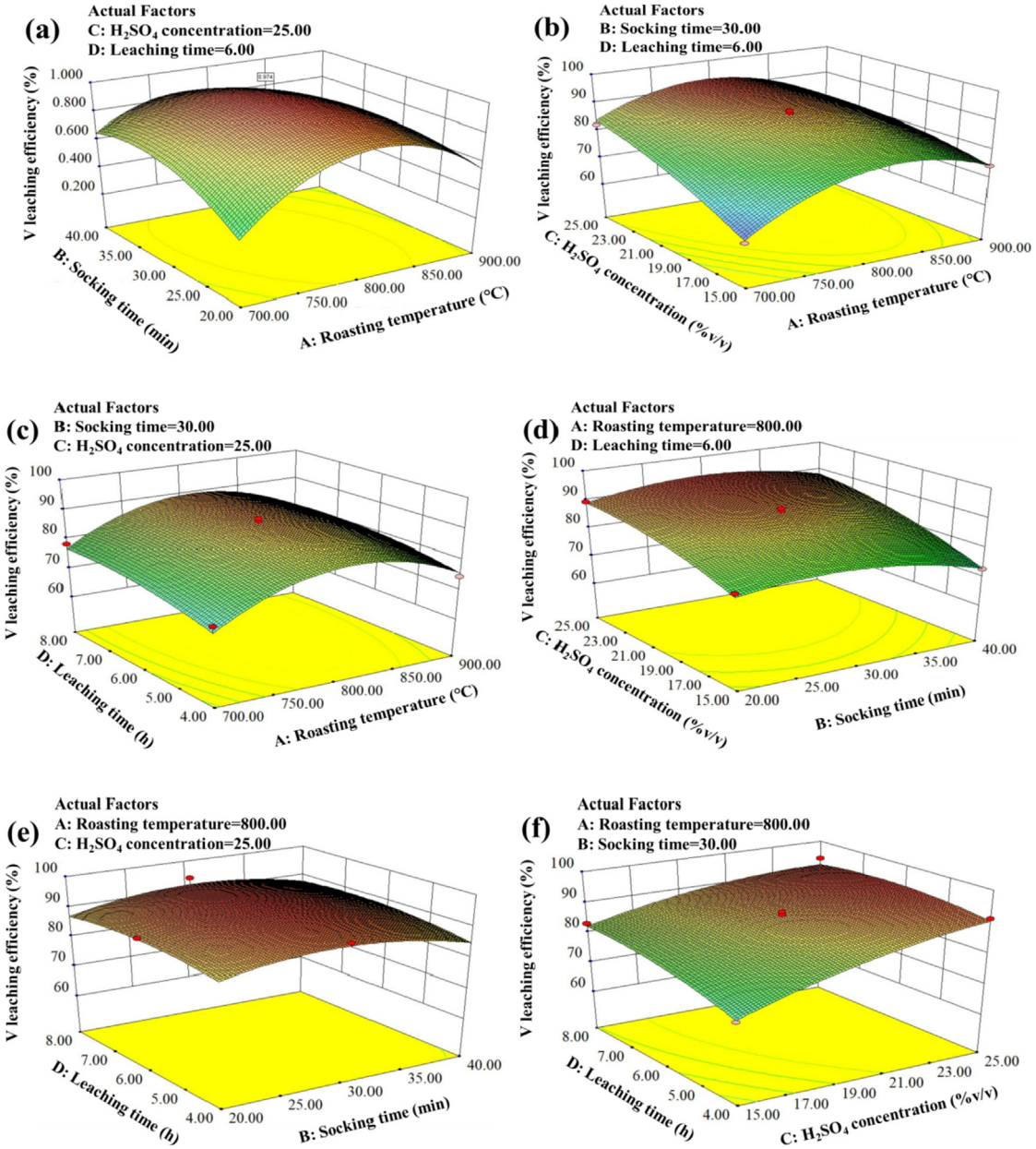


**Fig. 2.** 3D response surface plots showing the combined effects of Roasting temperature and Socking time (a), Roasting temperature and $H_2SO_4$ concentration (b), Roasting temperature and Leaching time (c), Socking time and $H_2SO_4$ concentration (d), Socking time and Leaching time (e), $H_2SO_4$ concentration and Leaching time (f).

**Table 4**
Optimized solutions generated by software.

| Number | A | B | C | D | Y | |
|---|---|---|---|---|---|---|
| 1 | 792.49 | 30.24 | 25.00 | 6.42 | 93.4 | |
| 2 | 792.41 | 30.20 | 25.00 | 6.41 | 93.4 | |
| 3 | 792.48 | 30.26 | 25.00 | 6.44 | 93.4 | |
| 4 | 792.63 | 30.33 | 25.00 | 6.42 | 93.4 | |
| 5 | 792.66 | 30.34 | 25.00 | 6.44 | 93.4 | |
| 6 | 792.05 | 30.38 | 25.00 | 6.41 | 93.4 | |
| 7 | 791.89 | 30.31 | 25.00 | 6.45 | 93.4 | |
| 8 | 792.05 | 30.22 | 25.00 | 6.46 | 93.4 | |
| 9 | 792.14 | 30.42 | 25.00 | 6.45 | 93.4 | |
| 10 | 792.87 | 30.37 | 25.00 | 6.46 | 93.4 | |
| 11 | 791.47 | 30.40 | 25.00 | 6.48 | 93.4 | |
| 12 | 791.37 | 30.08 | 25.00 | 6.38 | 93.4 | |
| 13 | 792.69 | 29.98 | 25.00 | 6.46 | 93.4 | |
| 14 | 790.09 | 30.44 | 25.00 | 6.44 | 93.4 | |
| 15 | 793.19 | 30.22 | 25.00 | 6.29 | 93.4 | |
| 16 | 791.48 | 30.48 | 25.00 | 6.57 | 93.4 | |
| 17 | 791.16 | 30.82 | 25.00 | 6.52 | 93.4 | |
| 18 | 795.04 | 29.76 | 25.00 | 6.51 | 93.4 | |
| 19 | 792.54 | 30.33 | 25.00 | 6.23 | 93.4 | |
| 20 | 794.32 | 30.40 | 25.00 | 6.58 | 93.4 | |
| 21 | 791.53 | 30.15 | 24.90 | 6.52 | 93.4 | |
| 22 | 793.26 | 30.66 | 25.00 | 6.75 | 93.4 | |
| 23 | 785.84 | 28.82 | 25.00 | 5.94 | 93.2 | Selected |
| 24 | 792.10 | 29.60 | 25.00 | 5.87 | 93.1 | |

parameters in MR-acid leaching process and CR-acid leaching process at similar V leaching efficiency level was presented in Table 5.

This was mainly due to the high efficiency of MR for microwave absorbent material. Due to the better effect of MR, V in microwave roasted samples leached more easily than in conventional roasted samples. These comparison data show that the microwave leaching process of V-bearing shale had lower energy consumption and better economic benefits than the conventional process. On the environmental side, MR equipment consumes electricity, while conventional roasters often need gas or coal for their operation; accordingly, there were no emissions from MR. In addition, to satisfy the subsequent leachate extraction process, it is necessary to adjust the pH of the leachate with an alkaline chemical. The neutralised slag produced is difficult to handle and has a high absorption capacity. As shown in Table 5, the MR acid leaching process consumes less sulphuric acid, which means that the neutralised slag produced in the subsequent process will be considerably reduced.

### 3.5. Strengthening mechanism of MR

#### 3.5.1. Promoting oxidation of low valent vanadium

In our previous work (Yuan et al., 2016), oxidation kinetics of V in shale during roasting process were investigated. The results showed that MR is more efficient in V oxidation. Fig. 3 shows the microscopic images of different roasted stone coal particles in the form of rock slice. In the same conditions, the internal black areas in MR particles are much looser and smaller than CR particles. Fig. 4

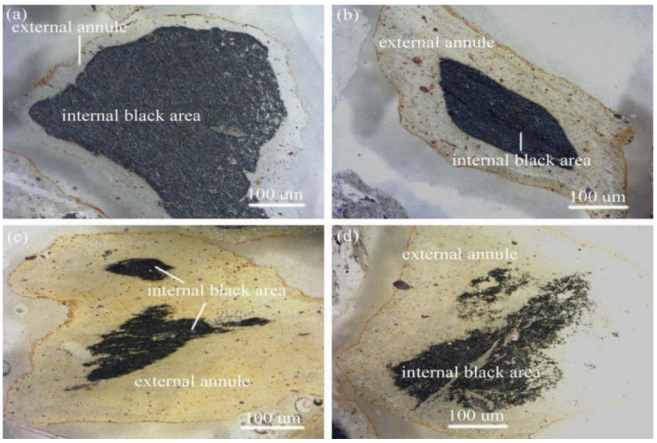


**Fig. 3.** Microscopic images of roasted samples in the form of a rock slice (Yuan et al., 2016). (a-CR600 °C/20 min; b-CR600 °C/30 min; c-MR600 °C/20 min; d-MR600 °C/30 min).

presents that the C and S contents in the internal black areas are much higher than the external light annular areas. It indicates that in the same conditions, MR has higher decarbonization and desulfurization efficiencies.

According to the material characterization, C and S are mainly come from coal and pyrite. As mentioned above, coal and pyrite are main microwave absorbing mediums in shale, hence coal and pyrite are highly active in microwave field. Furthermore, selective thermal effect triggers thermal stress, resulting in cracking of roasted particles, which facilitates mass transfer of gaseous products. Therefore, high activation and good mass transfer effect bring better decarbonization and desulfurization efficiencies for MR, which promotes oxidation of low-valent V.

#### 3.5.2. Promoting structural distortion of muscovite

In roasting process, dehydroxylation causes structural distortion of muscovite which is helpful for V extraction. In Fig. 6, $Z^{O}_{TOT}$ represents the spacing of the entire TOT unit along the C axis, $Z^{O}_{O}$ represents the spacing of Al—O(OH) octahedral structure layer, $T_{Si\text{-}O\alpha}$ represents the length of the Si—O bond along the c axis in the Si—O tetrahedron, $T_{Al\text{-}O\alpha}$ represents the length of the Al—O bond along the c axis in the Al—O tetrahedron. The structural parameters along the c axis of TOT units of muscovite before and after dehydroxylation were calculated using DFT and the results are showed in Table 6. After dehydroxylation, $Z^{O}_{TOT}$ increases by 0.013 nm, $Z^{O}_{O}$ increases by 0.017 nm, while $T_{Si\text{-}O\alpha}$ and $T_{Al\text{-}O\alpha}$ all decrease. It indicates that dehydroxylation increases the spacing of Al—O(OH) octahedral structure layer and decreases the spacing of Si(Al)—O tetrahedron structure layer. That means dehydroxylation weakens the energy of Al—O bond in octahedral structure and enhances the energy of Si(Al)—O bond in tetrahedron structure. As mentioned above, most V in shale exists in octahedral structure replacing Al. Therefore, dehydroxylation actually promotes the release of V from structure.

**Table 5**
Comparison of the main parameters in MR-acid leaching process and CR-acid leaching process.

| | Roasting equipment | Roasing Power | Running time (whole roasting process) | Roasting energy consumption | Leaching $H_2SO_4$ concentration | Leaching time | Leaching energy consumption (SZCL-2A type stirrer: 0.21 kW) |
|---|---|---|---|---|---|---|---|
| MR | HAMiLab-V | 1 kW | 38 min | 0.63 kW h | 25%v/v | 6 h | 1.26 kW h |
| CR | SX2-10-13 | 10 kW | 162.5 min | 27.08 kW h | 35%v/v | 10 h | 2.1 kW h |
| MR/CR | / | 10% | 23.38% | 2.3% | 71.43% | 60% | 60% |

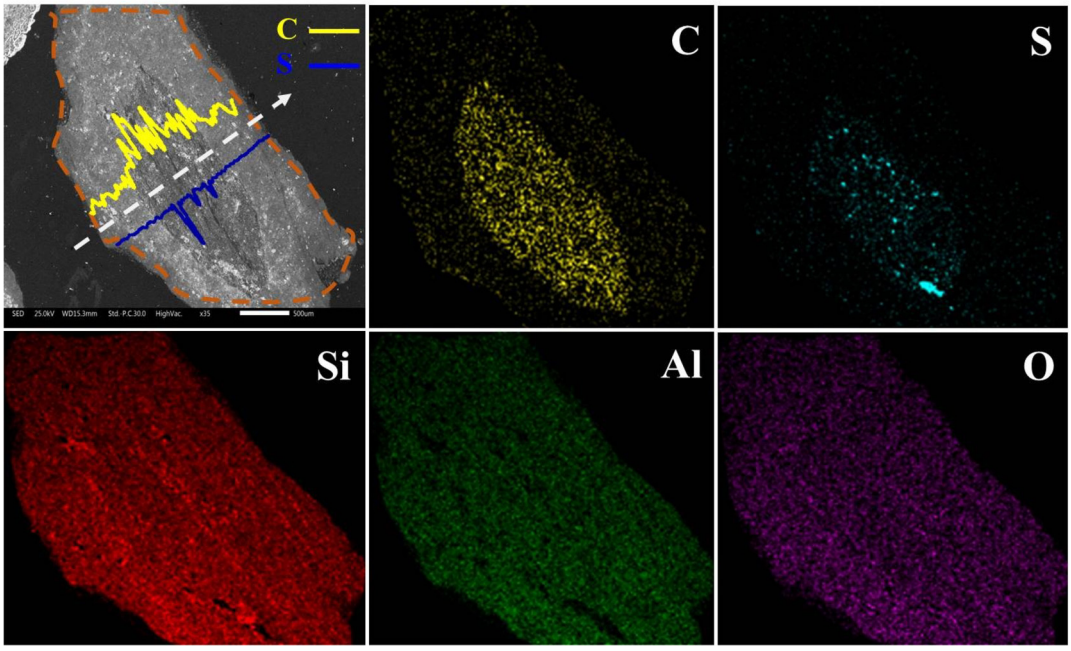


**Fig. 4.** SEM-EDS analysis of the cross section of a roasted particle.

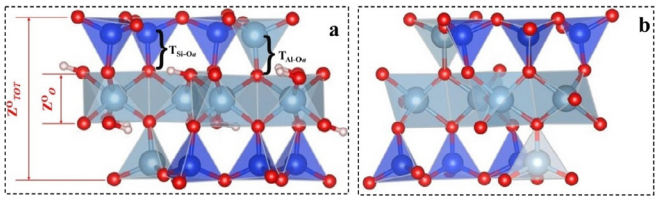


**Fig. 5.** TOT units of muscovite before and after dehydroxylation (a-before dehydroxylation; b-after dehydroxylation).

Fig. 6 shows the FTIR analyses of pure muscovite via different roasting methods. Bond 3626 $cm^{-1}$, 927 $cm^{-1}$ and 827 $cm^{-1}$ represent stretching vibration peaks of hydroxyl group. At 200 °C, the patterns of two roasting methods were almost identical. At 400 °C, bond 3626 $cm^{-1}$ 927 $cm^{-1}$ and 827 $cm^{-1}$ weaken slightly in MR pattern, which indicates dehydroxylation was gradually happening in microwave field. However, there was almost no change occurred in CR. At 600 °C, hydroxyl group peaks in CR pattern begin to weaken, but in MR pattern, there has been a marked decline of bond 3626 $cm^{-1}$ and bond 927 $cm^{-1}$, 827 $cm^{-1}$ had already disappeared. When temperature reached to 800 °C, all hydroxyl group peaks in MR pattern have disappeared, while there was still weak bond 3626 $cm^{-1}$ in CR pattern. As analysed above, MR had an absolute advantage in the dehydroxylation of muscovite comparing with CR. As we known, muscovite is not a microwave absorbing medium, but hydroxyl group is a typical polar group. Therefore, the hydroxyl group in muscovite has strong response to microwave and this response is selective for the other groups in muscovite structural.

Furthermore, the roasted pure muscovite were analysed using XRD, the results are showed in Fig. 7. With the increase of temperature, intensities of the diffraction peaks representing crystal surface in c axis decreased gradually and shifted to low angle. Normally, low angle migration of a diffraction peak means the spacing increased of corresponding crystal surface (Gridi-Bennadji et al., 2008). Based on the XRD analysis data, parameters of diffraction peak intensity, diffraction angle and crystal surface spacing for (006) crystal surface in different roasting methods were calculated via Prague formula (Jia et al., 2017) and presented in Table 6. In the same conditions, pure muscovite in MR had more obvious expansion along the c axis. According to the spacing relation between different parts in Table 7, it can be calculated that at 800 °C, spacing expansion of Al–O(OH) octahedral structure layer in MR was 0.036 nm and 0.026 nm in CR resulting the Al and V in octahedral structure had much higher reactive activity.

$\triangle d$ is the spacing change of (006) crystal surface, which is three times as the spacing of TOT unit (Qiu et al., 1998).

Based on the above characterizations and calculations, the enhancement mechanism of MR can be summarily expressed as follows: On the one hand, as strong microwave absorbing mediums, coal and pyrite are more active and have faster heating efficiencies than other minerals in shale. Selective thermal effect of MR triggers thermal stress, resulting in cracking of particles, which facilitates mass transfer of gaseous products. High activation and good mass transfer effect bring better decarbonization and desulfurization efficiencies for MR, which promotes oxidation of low-valent V. On the other hand, due to selective response to microwave of hydroxyl group, MR has an absolute advantage in dehydroxylation of muscovite, resulting the spacing expansion of Al–O(OH) octahedral structure layer as about 1.3 times as that of CR and significantly enhancing the release of V.

## 4. Conclusions

Based on the conditions optimized via RSM, a 93.4% V leaching efficiency can be obtained at MR temperature of 785 °C, MR time of 28 min, $H_2SO_4$ concentration of 25%v/v and leaching time of 6 h. Compared with CR-acid leaching under the condition of similar leaching efficiency, roasting temperature is reduced by 115 °C, roasting time is reduced by 32 min, $H_2SO_4$ concentration is reduced by 10%v/v and leaching time is reduced by 4 h. High activations of coal and pyrite and good mass transfer effect resulted by selective

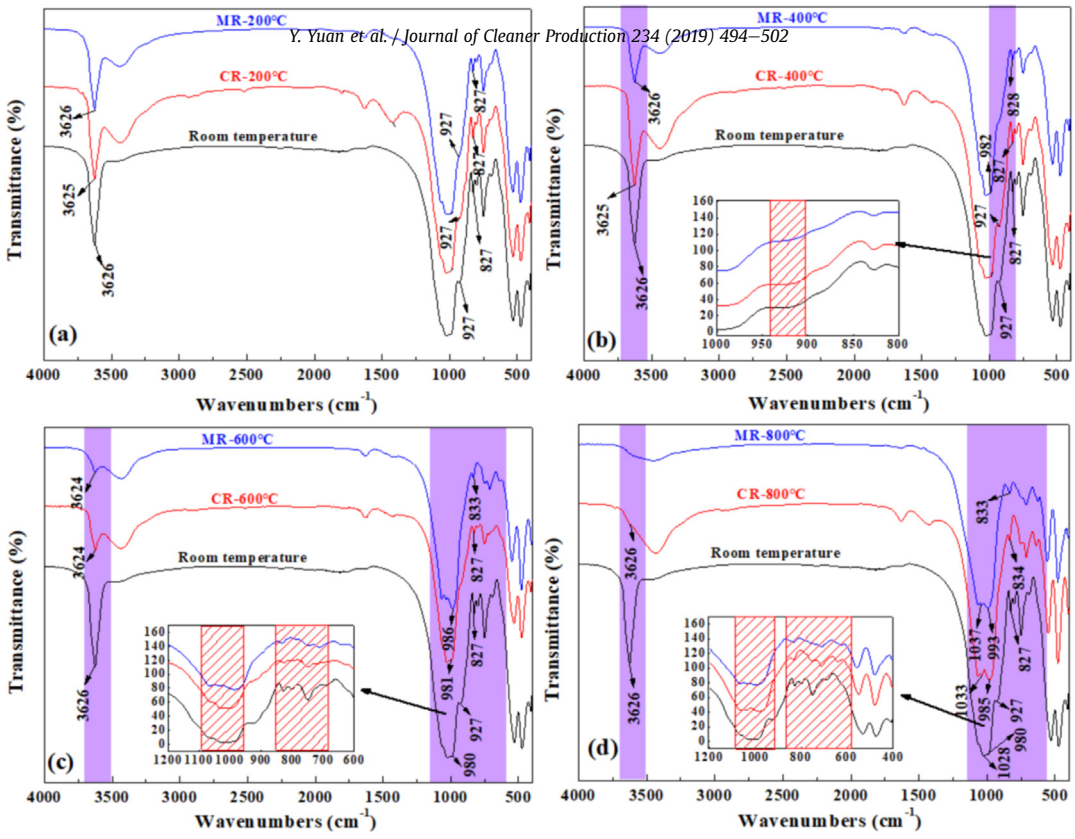


**Fig. 6.** FTIR analyses of pure muscovite via different roasting methods. (MR-microwave roasting; CR-conventional roasting; a-200 °C; d-400 °C; c-600 °C; d-800 °C).

**Table 6**
Structural parameters along the c axis of TOT units of muscovite before and after dehydroxylation.

| | Muscovite | Dehydroxylate muscovite |
|---|---|---|
| $Z^{O}_{TOT}$ | 0.68866 | 0.70195 |
| $Z^{O}_{O}$ | 0.21979 | 0.23677 |
| $T_{Si\text{-}O\alpha}$ | 0.16415 | 0.16345 |
| $T_{Al\text{-}O\alpha}$ | 0.17577 | 0.17455 |

thermal effect bring better decarbonization and desulfurization efficiencies for MR, which promotes oxidation of low-valent V. Because of selective response to microwave of hydroxyl group, MR is more excellent in dehydroxylation of muscovite, resulting the spacing expansion of Al–O(OH) octahedral structure layer as about 1.3 times as that of CR and significantly enhancing the release of V.

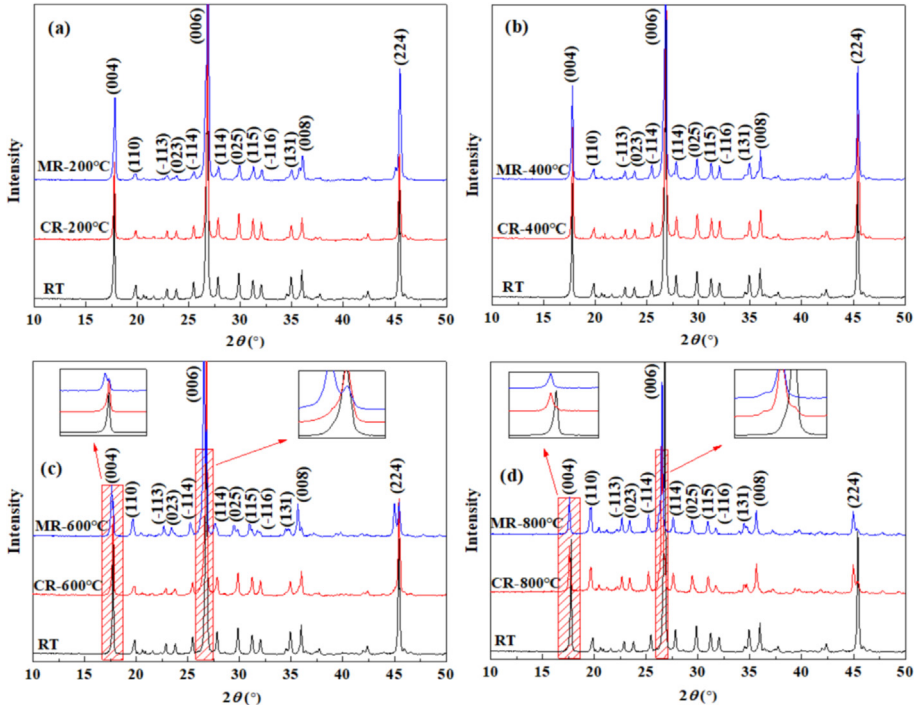


**Fig. 7.** XRD analyses of pure muscovite via different roasting methods (MR-microwave roasting; CR-conventional roasting; a-200 °C; d-400 °C; c-600 °C; d-800 °C).

**Table 7**
Parameters for (006) crystal surface in different roasting methods.

| Temperarure (°C) | CR-Intensity (cps) | CR-2$\theta$ (°) | CR-$\triangle d$ (nm) | MR-Intensity (cps) | MR-2$\theta$ (°) | MR-$\triangle d$ (nm) |
|---|---|---|---|---|---|---|
| RT | 11999 | 26.8151 | 0 | 11999 | 26.8151 | 0 |
| 200 | 11997 | 26.8151 | 0 | 10905 | 26.8145 | 2.12E-5 |
| 400 | 9402 | 26.8145 | 2.12E-5 | 7910 | 26.7823 | 1.94E-3 |
| 600 | 8007 | 26.7823 | 1.16E-3 | 7829 | 26.5528 | 9.38E-3 |
| 800 | 6756 | 26.5856 | 8.19E-3 | 5304 | 26.5201 | 1.06E-2 |

## Acknowledgements

This study was supported by the Project of National Natural Science Foundation of China (No.51774216).

## References

Asomaning, J., Haupt, S., Chae, M., Bressler, D.C., 2018. Recent developments in microwave-assisted thermal conversion of biomass for fuels and chemicals. Renew. Sustain. Energy Rev. 92, 642–657.
Choi, I.H., Moon, G., Lee, J.Y., Jyothi, R.K., 2018. Extraction of tungsten and vanadium from spent selective catalytic reduction catalyst for stationary application by pressure leaching process. J. Clean. Prod. 197, 163–169.
Fu, Z.B., 2009. The experimental research on extraction of vanadium from stone coal by no-salt-roasting and low acid leaching. Metal. Mine 399, 78–80, 112.
Forster, J., Pickles, C.A., Elliott, R., 2015. Microwave carbothermic reduction roasting of a low grade nickeliferous silicate laterite ore. Miner. Eng. 88, 18–27.
Ghafarzadeh, M., Abedini, R., Rajabi, R., 2017. Optimization of ultrasonic waves application in municipal wastewater sludge treatment using response surface method. J. Clean. Prod. 150, 361–370.
Gridi-Bennadji, F., Beneu, B., Laval, J.P., Blanchart, P., 2008. Structural transformations of Muscovite at high temperature by X-ray and neutron diffraction. Appl. Clay Sci. 38, 259–267.
Haque, K.E., 1999. Microwave energy for mineral treatment processes—a brief review. Int. J. Miner. Process. 57, 1–24.
Hu, P.C., Zhang, Y.M., Liu, T., Huang, J., Yuan, Y.Z., Xue, N.N., 2018a. Eco-Friendly leaching and separation of vanadium over iron impurity from vanadium-bearing shale using oxalic acid as a leachant. ACS Sustain. Chem. Eng. 6, 1900–1908.
Hu, P.C., Zhang, Y.M., Liu, T., Huang, J., Yuan, Y.Z., Xue, N.N., 2018b. Source separation of vanadium over iron from roasted vanadium bearing shale during acid leaching via ferric fluoride surface coating. J. Clean. Prod. 181, 399–407.
Hu, Y.J., Zhang, Y.M., Bao, S.X., Liu, T., 2012. Effects of the mineral phase and valence of vanadium on vanadium extraction from stone coal. Int. J. Miner. Metall. Mater. 19 (10), 893–898.
Jia, F.F., Yang, B.Q., Wan, Q., Song, S.X., 2017. Variation of interlayer binding energy of muscovite in its swelling. Comput. Mater. Sci. 132, 74–80.
Kaewwichit, P., Junsomboon, J., Chakartnarodom, P., Tippayasam, C., Srichumpong, T., Thavorniti, P., Leonelli, C., Chaysuwan, D., 2017. Development of microwave-assisted sintering of Portland cement raw meal. J. Clean. Prod. 142, 1252–1258.
Lee, C.S., Binner, E., Winkworth-Smith, C., John, R., Gomes, R., Robinson, J., 2016. Enhancing natural product extraction and mass transfer using selective microwave heating. Chem. Eng. Sci. 149, 97–103.
Li, J., Zhang, Y.M., Du, D.Y., Liu, Z.Y., 2017. Improvements in the decision making for Cleaner Production by data mining Case study of vanadium extraction industry using weak acid leaching process. J. Clean. Prod. 143, 582–597.
Li, J., Zhang, Y.M., Liu, T., Huang, J., Bao, S.X., 2014. A methodology for assessing cleaner production in the vanadium extraction industry. J. Clean. Prod. 84, 598–605.
Li, R.M., Liu, T., Zhang, Y.M., Huang, J., Xu, C.B., 2018. Efficient Extraction of vanadium from vanadium–titanium magnetite concentrate by potassium salt roasting additives. Minerals 8, 25.
Liu, Y.H., Yang, C., Li, P.Y., Li, S.Q., 2010. A new process of extracting vanadium from stone coal. Int. J. Miner. Metall. Mater. 17 (4), 381–388.
Markandeya Dhiman, N., Shukla, S.P., Kisku, G.C., 2017. In: Statistical Optimization of Process Parameters for Removal of Dyes from Wastewater on Chitosan Cenospheres Nanocompodsite Using Response Surface Methoology, vol. 149, pp. 597–606.
Mohammed, I.Y., Abakr, Y.A., Yusup, S., Kazi, F.K., 2017. Valorization of Napier grass via intermediate pyrolysis: optimization using response surface methodology and pyrolysis products characterization. J. Clean. Prod. 142, 1848–1866.
Qiu, L., Hu, Y.H., 1998. X Ray Diffraction Technology and Equipment. Metallurgical industry press, Beijing, pp. 13–14.
Ranic, M., Nikolic, M., Pavlovic, M., Buntic, A., Siler-Marinkovic, S., Dimitrijevic-Brankovic, S., 2014. Optimization of microwave-assisted extraction of natural antioxidants from spent espresso coffee grounds by response surface methodology. J. Clean. Prod. 80, 69–79.
Wang, C.Q., Wang, H., Liu, Y.N., Huang, L.L., 2016. Optimization of surface treatment for flotation separation of polyvinyl chloride and polyethylene terephthalate waste plastics using response surface methodology. J. Clean. Prod. 139, 866–872.
Wang, F., Zhang, Y.M., Liu, T., Huang, J., Zhao, J., Zhang, G.B., Liu, J., 2015. A mechanism of calcium fluoride-enhanced vanadium leaching from stone coal. Int. J. Miner. Process. 145, 87–93.
Wang, F., Zhang, Y.M., Liu, T., Huang, J., Zhao, J., Zhang, G.B., Liu, J., 2014. Comparison of direct acid leaching process and blank roasting acid leaching process in extracting vanadium from stone coal. Int. J. Miner. Process. 128, 40–47.
Wang, K.Y., Dimitrakis, G., Irvine, D.J., 2017. Exemplification of catalyst design for microwave selective heating and its application to efficient in situ catalyst synthesis. Chem. Eng. Process 122, 389–396.
Wang, W.K., Wang, F.C., Lu, F.H., 2018. Microwave alkaline roasting-water dissolving process for germanium extraction from zinc oxide dust and its analysis by response surface methodology (RSM). Metall. Res. Technol. 115, 203–212.
Xue, N.N., Zhang, Y.M., Liu, T., Huang, J., Zheng, Q.S., 2017. Effects of hydration and hardening of calcium sulfate on muscovite dissolution during pressure acid leaching of black shale. J. Clean. Prod. 149, 989–998.
Yuan, Y.Z., Zhang, Y.M., Liu, T., Chen, T.J., Huang, J., 2016. Comparison of microwave and conventional blank roasting and of their effects on vanadium oxidation in stone coal. J. Microw. Power Electromagn. Energy 2 (50), 81–93.
Yuan, Y.Z., Zhang, Y.M., Liu, T., Chen, T.J., 2017. MR with size grading based on the influence of carbon on vanadium extraction from stone coal via MR-acid leaching. RSC Adv. 7, 1387.
Zhang, X.Y., Qin, W.Q., Tian, X.D., Chen, Y.B., Gu, Y., Xi, X.G., 2011. MR-acidic leaching technique for extraction of vanadium from stone coal. Chin. J. Nonferrous Metals 21, 908–912.
Zhang, Y.M., Bao, S.X., Liu, T., Chen, T.J., Huang, J., 2011. The technology of extracting vanadium from stone coal in China: history, current status and future prospects. Hydrometallurgy 109, 116–124.
Zhang, Y.M., Zhu, X.B., Liu, T., Huang, J., Song, S.X., 2013. Effect of colloidal potassium alum formation on vanadium recovery from acid leach solutions of stone coal. Hydrometallurgy 138, 54–58.
Zheng, Q.S., Zhang, Y.M., Liu, T., Huang, J., Xue, N.N., Shi, Q.H., 2017. Optimal location of vanadium in muscovite and its geometrical and electronic properties by DFT calculation. Minerals 7, 32.
Zhu, X.B., Zhang, Y.M., Huang, J., Liu, T., Li, W., 2012. A kinetics study of multi-stage counter-current circulation acid leaching of vanadium from stone coal. Int. J. Miner. Process. 114–117, 1–6.
Zhu, Y.G., Zhang, G.F., Feng, Q.M., Lu, Y.P., Ou, L.M., Huang, S.J., 2010. Acid leaching of vanadium from roasted residue of stone coal. Trans. Nonferrous Metals Soc. China 20, s107–s111.